

Mechanical behavior of rock-coal-rock specimens with different coal thicknesses

Wei-Yao Guo^{1,2}, Yun-Liang Tan^{*1,2}, Feng-Hai Yu^{**1,2}, Tong-Bin Zhao^{1,2},
Shan-Chao Hu^{1,2}, Dong-Mei Huang^{1,2} and Zhe Qin²

¹State Key Laboratory of Mining Disaster Prevention and Control Co-founded by Shandong Province and the Ministry of Science and Technology, Shandong University of Science and Technology, Qingdao 266590, China

²National Demonstration Center for Experimental Mining Engineering Education, Shandong University of Science and Technology, Qingdao 266590, China

(Received February 28, 2017, Revised January 11, 2018, Accepted January 26, 2018)

Abstract. To explore the influence of coal thickness on the mechanical behavior and the failure characteristics of rock-coal-rock (RCR) mass, the experimental investigation of uniaxial compressive tests was conducted first and then a systematic numerical simulation by particle flow code (PFC2D) was performed to deeply analyze the failure mechanical behavior of RCR specimens with different coal thicknesses in conventional compression tests. The overall elastic modulus and peak stress of RCR specimens lie between the rock and the coal. Inter-particle properties were calibrated to match the physical sample strength and the stiffness response. Numerical simulation results show that the deformation and strength behaviors of RCR specimens depend not only on the coal thickness, but also on the confining pressure. Under low confining pressures, the overall failure mechanism of RCR specimen is the serious damage of coal section when the coal thickness is smaller than 30 mm, but it is shear failure of coal section when the coal thickness is larger than 30 mm. Whereas under high confining pressures, obvious shear bands exist in both the coal section and the rock section when the coal thickness is larger than 30 mm, but when the coal thickness is smaller than 30mm, the failure mechanism is serious damage of coal section and shear failure of rock section.

Keywords: rock mechanics; RCR combined body; particle flow; confining pressure; failure; mechanical behavior

1. Introduction

The geotechnical properties of rock associated with coal seams play a significant role in the design, operation, and safety of underground and open-cut mining operations, especially the mechanical behavior of combined structure composed of coal and rock masses reflects the combination of coal, rock and interface at different loading conditions. Instability may directly reflect the dynamic disaster, such as roof fall and rock burst (Song *et al.* 2015, Panaghi *et al.* 2015, Chen *et al.* 2016, Huang *et al.* 2017, Guo *et al.* 2017a, Lin *et al.* 2017, Zhao *et al.* 2018, Zhang *et al.* 2018). The nature of the coal-rock itself dominates in the geo-mechanical behavior, and its geotechnical properties have been evaluated by extensive geo-mechanical tests (Chen *et al.* 2012, Bukowska 2013, Guo *et al.* 2017b, Tan *et al.* 2017, Lin *et al.* 2016). A comprehensive understanding of the mechanical behavior of the combined coal-rock mass is therefore essential in assessing the potential dynamic hazard before, during and after the mining process. In the process of deep coal exploitation, engineering accidents and disasters often occur due to the instability and the failure of

the coal and rock structure (Kaiser *et al.* 2012, Meng *et al.* 2015, Tan *et al.* 2015, Zhao *et al.* 2017a, Ning *et al.* 2017). It is known that coal-rock dynamic disasters can be easily induced when the roof and the floor suddenly lose stability in the process of coal mining (Lu *et al.* 2015). Therefore, the interaction between the surrounding rock and coal is one of the key factors to keep the dynamic equilibrium of structure of roof, coal and floor.

In recent years, scholars have conducted significant work on the structure of combined coal-rock mass, and some achievements have been obtained. For example, Gale (1998) and Newman (2002) found that the designed coal pillar has a potential to expand laterally and that the frictional force developed along roof-coal and coal-floor interfaces is very important to rock burst. Vakili and Hebblewhite (2010) developed a new cavability assessment criterion for longwall top caving in combined coal-rock system composed of roof, top coal, cutting coal, and floor based on the numerical model. Sherizadeh *et al.* (2016) and Duncan (2000) examined the effect of different geological and mining factors on roof and coal stability in underground coal mines by combining field observations, laboratory testing, and numerical modeling. Liu *et al.* (2013) studied the synergistic instability of coal pillar and roof system and filling method based on plate model (i.e., a mechanical model of the elastic plate is based on plate bending theory), and found that box-filling can control ground subsidence, mine flood and mine fire efficiently. Zuo (2011) and Zhang *et al.* (2012) found that the failure of combined coal-rock

*Corresponding author, Professor
E-mail: yunliangtan@163.com

**Corresponding author, Ph.D.
E-mail: yufenghai2006@163.com

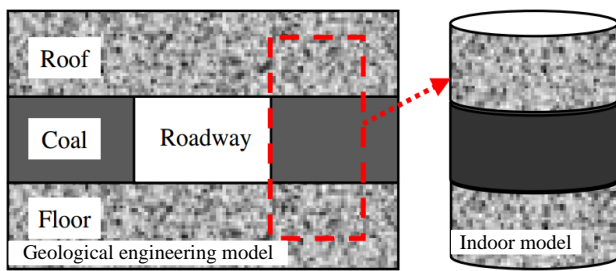


Fig. 1 RCR combined body concept model (Zuo *et al.* 2013)

mass mainly occurs within the coal, and that confining pressure, combination mode, and loading condition play an essential role on its failure mechanism. Poulsen *et al.* (2014) studied the strength reduction of a coal pillar due to water saturation embedded in combined structure composed of roof, coal pillar and floor using numerical model. Wang *et al.* (2014) developed a test system to understand the sliding mechanism of coal-rock structure, and revealed that sliding types have close relation with the axial loads and loading rates. Zhao *et al.* (2015a) developed a compressive-shear strength criterion of the rock-coal combination model considering interface effect. Guo (2011) and Zhao *et al.* (2016) investigated the mechanical characteristics and the failure mechanism of combined coal-rock specimens with different interfacial angles. He *et al.* (2011), Rafael *et al.* (2010), and Takeuchi *et al.* (2006) analyzed the deformation and fracture behavior of coal-rock combination body and obtained the precursor information of failure by means of acoustic-electric effect. Wang *et al.* (2016) studied the rock burst tendencies, failure characteristics, and charge induction laws during the failure process of coal-rock bodies through experimental investigations.

Generally, the design of roadways is gradually being transferred from rock roadways to coal roadways because the large-scale high intensity coal exploitation and the continuing improvement in the coal exploitation technology. As shown in Fig. 1, the stability of roadways in coal seams at large mining depth depends greatly on the overall failure properties of the RCR combined body under high stress conditions. Although scholars have done extensive researches on the coal roadway stability for decades, only a small amount of literature attempted to study the mechanical behavior of RCR specimens, especially a comprehensive study of RCR specimens with different coal thicknesses under conventional compression conditions. For example, Zuo *et al.* (2013) analyzed the failure behavior of one type of RCR specimens; and Huang *et al.* (2013) studied the effect of loading rate on the mechanical behavior of RCR specimens.

The method of particle flow simulation can effectively reflect the microstructure characteristics and essentially reveal the mechanism of the rock deformation and the failure (Zhao *et al.* 2017b). In this paper, experimental investigation of uniaxial compressive tests for RCR, rock, and coal specimens was conducted first and then a systematic numerical simulation by PFC2D (i.e., Particle Flow Code software which is two dimensional proposed by

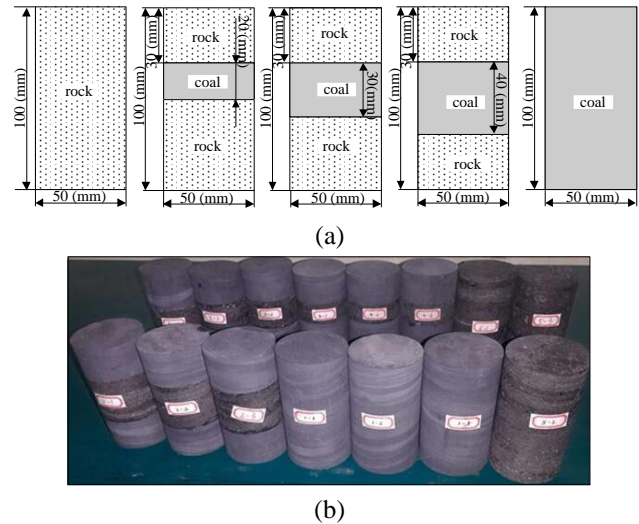


Fig. 2 Composition of RCR specimens (a) Sizes of specimens and (b) Test specimens

Potyondy and Cundall (2004)) was performed to analyze the failure mechanical behavior of RCR specimens with different coal thicknesses under conventional compression tests. The objective is to reveal the influence of the coal thickness on the deformation, strength, and failure mode of RCR mass, further, to reveal the failure mechanism. The work is expected to provide some references to clarify the mechanical properties and the instability failure mechanism of RCR mass with different coal thicknesses during the extraction process of coal resources.

2. Experimental investigation on the failure mechanical behavior of RCR specimens with different coal thicknesses under uniaxial compressive tests

2.1 Specimen preparation and testing procedure

2.1.1 Specimen preparation

The coal and rock (immediate roof) studied here were taken from the same working face in Mine A. The working face was located in the No. 10 coal seam at the depth ranging from 920 m to 1047 m below the ground surface. The rock was siltstone, which was grey black and medium thick layered rock. The coal and rock blocks were wrapped with multiple plastic membranes so as to retain their original state.

The specimens were selected for this research without any damage after they were processed in various heights according to the test plan. Then, these specimens are combined into a standard composed RCR specimen with diameter and height of 50 mm and 100 mm in proper order with superglue, as show in Fig. 2. The process precision of specimens (parallelism, flatness and verticality) was in compliance with the requirements of ISRM. The selected specimens were placed into an incubator so that all specimens were under the condition of identical relative humidity. In addition, the room temperature was kept consistent during the testing so as to eliminate the impacts

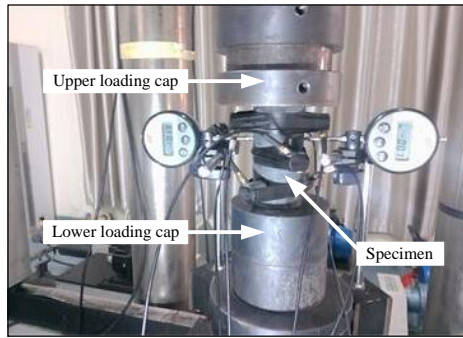


Fig. 3 Testing system

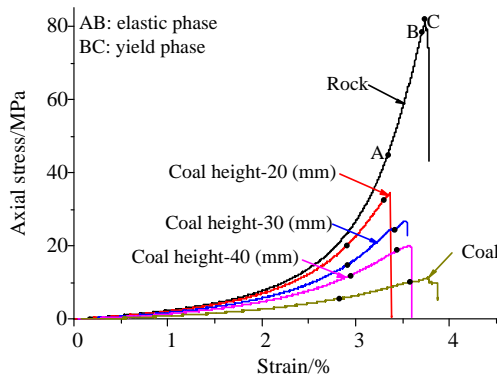


Fig. 4 Overall stress-strain curves of coal, rock, and RCR specimens under uniaxial compressive tests

of humidity, temperature and other factors.

2.1.2 Test equipment and procedure

The uniaxial compressive tests were all conducted on a RLJW-2000 servo-controlled rock pressure testing machine at the College of Mining and Safety Engineering, Shandong University of Science and Technology, as shown in Fig. 3. This testing system can record stress and strain data automatically. All specimens were loaded at the strain rate of 0.005 mm/s. The uniaxial compressive tests were carried out under a natural state (room temperature and humidity). To obtain the mechanical behaviors with the change of coal thickness under uniaxial compressive tests, five test schemes were designed. The heights of the coal were 0 mm (pure rock specimen), 20 mm, 30 mm, 40 mm, and 100 mm (pure coal specimen) respectively, as show in Fig. 2. In order to ensure the data accuracy, the number of test specimens for each scheme was not less than three, and the valid data was chosen as the test results for further analysis.

2.2 Experimental results of RCR specimens with different coal thicknesses under uniaxial compressive tests

2.2.1 Overall stress-strain curves

The overall stress-strain curves of the coal, the rock, and RCR specimens with different coal thicknesses are compared in Fig. 4. The overall stress-strain curves of RCR specimens are similar to that of the pure coal or rock specimen, including phases of the compaction, the elastic deformation, the plastic deformation and the failure. In the

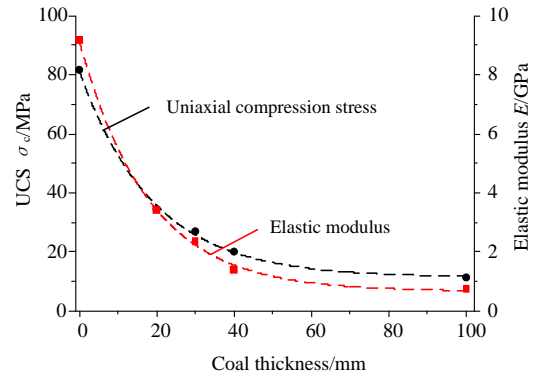


Fig. 5 Influence of coal thickness on the uniaxial compressive strength and elastic modulus under uniaxial compression tests

linear elastic phase, it shows clearly that the overall elastic modulus of RCR specimens lies between rock and coal. The yield phase is influenced by the variation of the coal thickness. The duration of yield phase decreases as the coal thickness decreases. Because of the loading method with load control and the mechanical properties, the failure duration of specimens is very short from the peak stress to the complete destruction.

Moreover, it is abnormal that the compaction of these specimens is greater in coal or rock. The reason is that the test equipment did not work well during that test period since that the air in the hydraulic oil could not been exhausted enough. In other words, the compaction phase included the deformation of air. The air was not compacted enough, leading to a hard application of the axial load, and as a result, the axial strain of compaction phase was greater. Fortunately, only the compaction phase was influenced, whereas the test results of USC, elastic modulus and failure modes were not influenced which were used for calibrating the micro-parameters of numerical models. Therefore, the influence of compaction phase could be ignored in this study.

2.2.2 Mechanical parameters

The influence of the coal thickness of RCR specimens on the uniaxial compressive strength (UCS) and the elastic modulus under uniaxial compressive tests is given in Fig. 5. Both the uniaxial compressive strength and the elastic modulus of RCR specimens increase with the decrease of the coal thickness. That is to say, the strength of the bearing capacity of coal strata will increase as the coal thickness decreases under the same engineering geology condition. Besides, it also reveals that when gate driving in the thin coal seam, the width of the plastic zone of coal wall may be smaller compared with thick coal seam due to the higher bearing capacity.

3. Numerical investigation on the failure mechanical behavior of RCR specimens with different coal thicknesses under conventional compression tests

3.1 Discrete element model

3.1.1 Micro-bond model

In PFC2D, there are two kinds of failure modes between particles, including shear failure and tension failure. PFC2D has two different bond models, including the contact bond model (CBM) and parallel bond model (PBM) generally used for simulating granular materials and compact materials, respectively. There are two advantages for PBM. On the one hand, parallel bonds can transmit both forces and moments between particles; on the other hand, bond breakage can lead to the immediate decrease in the macro stiffness. It is generally acknowledged that rock is porous material composed of mineral particles of different sizes and shapes, and these particles are bonded together by cement (Tan *et al.* 2016). Under conventional loading conditions, the failure modes of rock include the splitting failure, the shear failure, the tensile failure and their combination at the macro level; but at the micro level, the failure modes of particles consist of shear and tensile failure. In other words, the macroscopic failure of rock is accompanied by the accumulation and coalescence of particles failure (micro-cracks). In PBM, the micro-properties of the material are described by the stiffness and strength parameters of particles and bonds. Tensile and shear cracks form from bond breakage between adjacent particles (Zhao *et al.* 2016). The accumulation and coalescence of micro-cracks lead to macroscopic failure of the numerical model. Therefore, PBM can be more realistic for simulating rock material. In this paper, we chose PBM to carry out the numerical simulation.

3.1.2 Numerical RCR specimen and simulation procedure

The height and the width of numerical specimen were 100 mm and 50 mm, respectively, which are similar to those of the experimental specimen. The numerical specimen was discretized into 11693 particles. The particle size followed a uniform distribution varying from 0.3 to 0.4 mm. The average unit of the coal and the rock were about 1800 kg/m³, and 2600 kg/m³, respectively. After generating the specimen, we established RCR specimens by grouping these ball particles. In the experimental study, we only designed three kinds of RCR specimens, because specimens were not enough and difficult in preparing. In order to investigate the influence of the coal thickness on the strength, deformation, and failure mechanisms of RCR specimens in detail, we designed six kinds of RCR specimens as shown in Fig. 6. The heights of coal (red ball particles) were 10 mm, 20 mm, 30 mm, 40 mm, 50 mm, and 60 mm, respectively. Detailed descriptions of RCR specimens with different coal thicknesses under compression tests are listed in Table 1. A series of conventional compression tests were carried out for RCR specimens with different coal thicknesses under different confining pressures, namely 0 MPa, 2 MPa, 5 MPa, 10 MPa, 15 MPa, and 20 MPa.

An external displacement was applied on the top of the specimens in the axial direction. The loading rate must be low to ensure the specimen remained in a quasi-static state throughout the simulation process. Zhang and Wong (2013) researched the influence of the loading rate on the mechanical behavior of specimens containing pre-fissures,

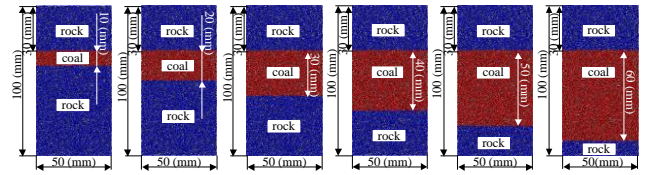


Fig. 6 Numerical specimens of RCR specimens with different coal thicknesses

Table 1 RCR specimens with different coal thicknesses under different confining pressure

Coal thickness (mm)	Coal ratio (%)	Rock ratio (%)	σ_3 (MPa)
10	10	90	0, 2, 5, 10, 15, and 20
20	20	80	0, 2, 5, 10, 15, and 20
30	30	70	0, 2, 5, 10, 15, and 20
40	40	60	0, 2, 5, 10, 15, and 20
50	50	50	0, 2, 5, 10, 15, and 20
60	60	40	0, 2, 5, 10, 15, and 20

Table 2 Micro-parameters of coal and rock

Micro-parameters	Coal	Rock
Elastic modulus of the particle, E_c (GPa)	0.45	6.5
Ratio of normal to shear stiffness of the particle, k_n/k_s	2.5	2.5
Ratio of normal to shear stiffness of the parallel bond, \bar{k}_n/\bar{k}_s	2.5	2.5
Particle friction coefficient, μ	0.5	0.5
Parallel-bond normal strength, σ_n (MPa)	9.9	70
Parallel-bond shear strength, τ_n (MPa)	9.9	70

which showed that the crack initiation stress and uniaxial compressive strength remained steady when the loading rate increased from 0.005 m/s to 0.08 m/s. Besides, Zhang *et al.* (2016) studied the influence of the loading rate on the mechanical behavior of the intact granite by PFC2D, and revealed that when the loading rate changes from 0.001 m/s to 0.05 m/s, the mechanical behavior of the granite changes slightly. Therefore, the loading rate of 0.05 m/s was chosen in this numerical simulation and the loading was applied until the failure occurred.

3.2 Confirmation for micro-parameters of coal and rock

3.2.1 Confirming method for micro-parameters

Determining the micro-parameters for numerical simulation is difficult by experiment. However, it is very essential to establish a correlation between macro-behavior and micro-parameters to validate the particle properties used in numerical specimens. The macro-behavior includes the axial strain curve, the peak stress, the elastic modulus, and the failure mode, etc. The trial and error method was used in confirming the micro-parameters. The macro-behavior of the coal specimen and the rock specimen obtained by experiment in Section 2 was used to calibrate the micro-parameters. After each trial, the macroscopic results obtained by numerical simulation were used to compare with the experimental results. This process was

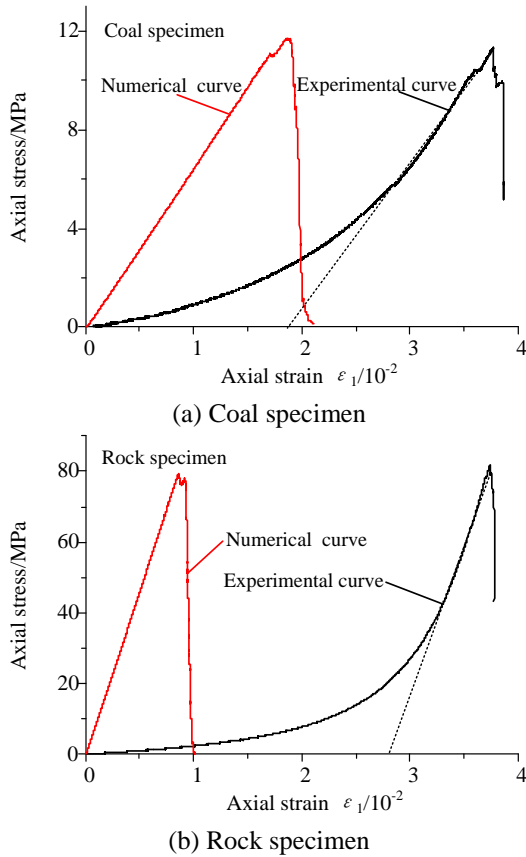


Fig. 7 Comparison between experimental and numerical stress-strain curves of coal and rock under uniaxial compression

repeated until the numerical results were similar to the experimental results. The micro-parameters used in PFC2D model for the coal and the rock are listed in Table 2.

3.2.2 Calibration of micro-parameters by experimental results

The comparison between experimental and numerical stress-strain curves under the uniaxial compression is shown in Fig. 7. From Fig. 7, it can be seen that both the numerically simulated curves and the experimental curves include the stage of elastic deformation, the stage of crack initiation and growth, and the stage of unstable failure. However, the experiment specimen also has a stage of compaction and nonlinear deformation at low stress levels, which are not observed in the numerical specimen. This is because the compaction stage is hard to be repeated in the numerical simulation.

The comparison of mechanical parameters between the experimental results and numerical results is listed in Table 3. In Table 3, σ_c is defined as the uniaxial compressive strength, and E refers to the slope of the linear part of the stress-strain curve. In accordance with Table 3, it shows clearly that the simulated peak stress and the elastic modulus are almost equal to those obtained by the experiment. The tensile strengths of numerical coal and rock specimens were also tested and were in the range of 5–20% of UCS, which are 1.79 MPa and 11.99 MPa, respectively.

Table 3 Comparison between the experimental and numerical mechanical parameters of coal and rock

Mechanical parameters	Experimental results		Numerical results	
	Coal	Rock	Coal	Rock
σ_c (MPa)	11.32	81.68	11.68	79.28
E (GPa)	0.74	9.17	0.71	9.31
σ_t (MPa)			1.79	11.99

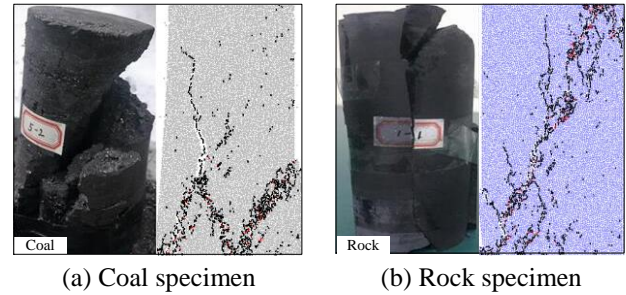


Fig. 8 Comparison between experimental and numerical failure modes of coal and rock under uniaxial compression tests (Note, the black and red dots represent the tensile micro-crack and shear micro-crack, respectively)

The comparison between the experimental and numerical failure modes of the coal and the rock is depicted in Fig. 8. Fig. 8 illustrates that the failure modes of coal and rock specimens are axial splitting under numerical simulation, which is similar to those obtained by the experiment. The comparisons shown in Figs. 7 and 8 calibrate the rightness and reasonability of micro-parameters used in Table 2.

3.3 Numerical results of RCR specimens with different coal thicknesses under conventional compression tests

3.3.1 Overall stress-strain curves

Axial deviatoric stress-axial strain curves of RCR specimens with different coal thicknesses under different confining pressures are shown in Fig. 9. From Fig. 9, we can conclude that the yield stress and the peak stress of RCR specimens increase gradually as the confining pressure increases, which will be analyzed in detail in the next section.

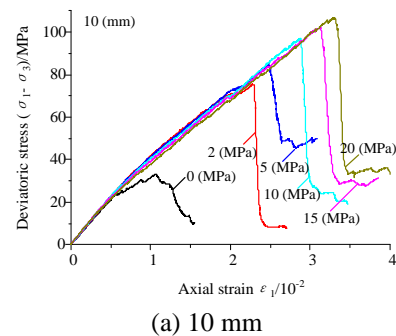


Fig. 9 Axial deviatoric stress-axial strain curves of RCR specimens with different coal thicknesses

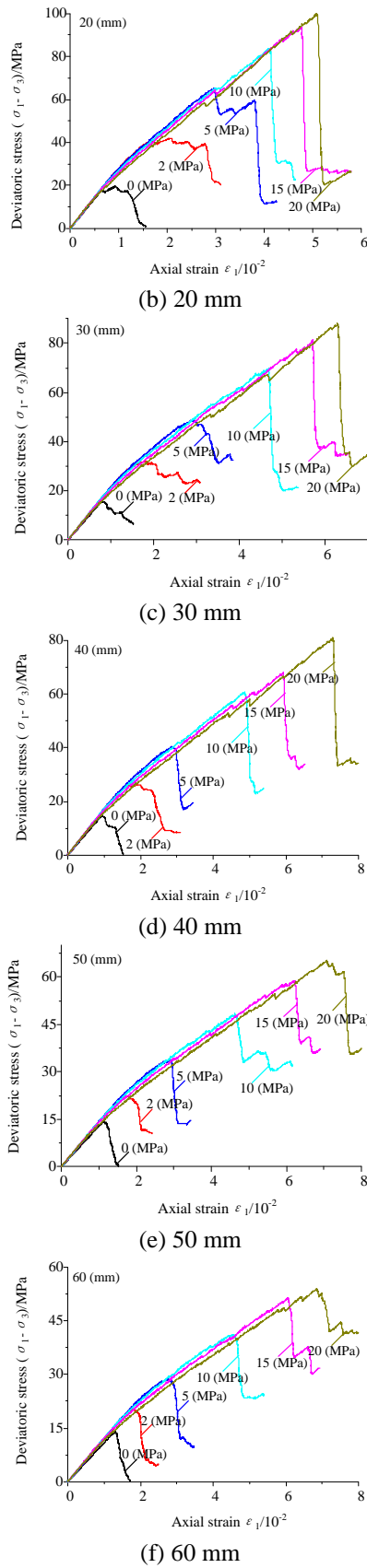


Fig. 9 Continued

Tables 4, 5 and 6 list the peak stress (σ_{1max}), the elastic modulus (E), and the peak axial strain (ϵ_{1max}) of RCR

Table 4 Peak stress (σ_{1max}) of RCR specimens with different coal thicknesses under compression tests (unit MPa)

σ_3 (MPa)	10 (mm)	20 (mm)	30 (mm)	40 (mm)	50 (mm)	60 (mm)
0	33.18	19.72	15.75	14.79	14.25	14.02
2	75.35	42.98	34.14	28.16	24.45	22.32
5	90.06	70.25	53.43	45.22	38.81	33.65
10	107.05	93.68	79.75	70.58	58.38	51.13
15	117.25	108.41	96.43	83.26	73.79	66.26
20	126.56	119.89	107.75	100.89	85.42	73.84

Table 5 Elastic modulus (E) of RCR specimens with different coal thicknesses under compression tests (unit GPa)

σ_3 (MPa)	10 (mm)	20 (mm)	30 (mm)	40 (mm)	50 (mm)	60 (mm)
0	4.33	2.77	2.04	1.62	1.32	1.1
2	4.42	2.89	2.16	1.71	1.4	1.2
5	4.48	2.92	2.2	1.75	1.43	1.22
10	4.48	2.94	2.24	1.76	1.45	1.24
15	4.49	2.89	2.21	1.75	1.43	1.22
20	4.42	2.92	2.19	1.74	1.39	1.18

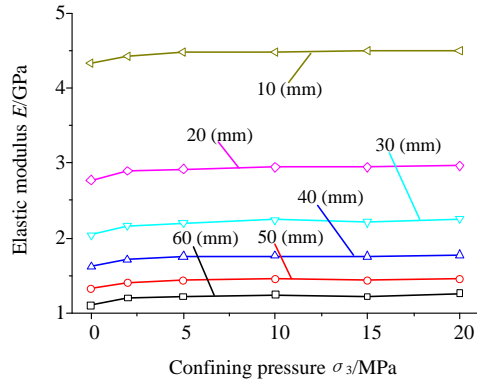
Table 6 Peak axial strain (ϵ_{1max}) of RCR specimens with different coal thicknesses under compression tests (unit 10^{-2})

σ_3 (MPa)	10 (mm)	20 (mm)	30 (mm)	40 (mm)	50 (mm)	60 (mm)
0	1.0714	0.9265	0.7909	0.9526	1.1474	1.3178
2	2.2928	2.0781	1.8087	1.6986	1.768	1.8274
5	2.4778	2.9688	2.9481	2.9102	2.8754	2.7205
10	2.8835	4.0737	4.6837	4.8636	4.6239	4.5825
15	3.1317	4.7597	5.7147	5.9323	6.23	6.0607
20	3.3032	5.0818	6.2897	7.2867	7.0772	6.8549

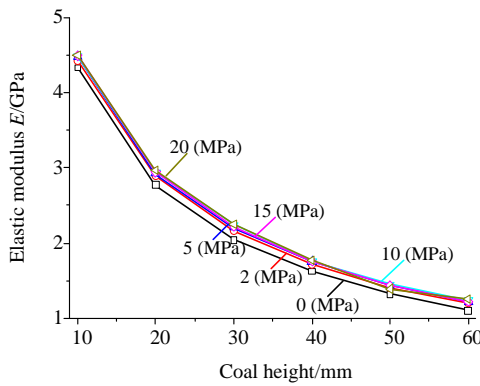
specimens with different coal thicknesses under different confining pressures, respectively. In accordance with the numerical results listed in Tables 4, 5, and 6, generally, the deformation and strength behaviors of RCR specimens are found depending not only on the coal thickness, but also on the confining pressure.

3.3.2 Effects of coal thickness on the deformation behavior of RCR specimens

Fig. 10(a) shows the influence of the confining pressure on the elastic modulus of RCR specimens with different coal thicknesses. From Fig. 10(a), it can be seen that for the same coal thickness, with the increase of confining pressure, the elastic modulus of RCR specimen all increases nonlinearly when the confining pressure is less than 5 MPa. Take the coal thickness of 40mm as an example, the elastic modulus of RCR specimen increases from 1.62 to 1.75 GPa as the confining pressure increases from 0 to 5 MPa. However, when the confining pressure is larger than 5 MPa, the elastic modulus of RCR specimen keeps almost steady as the confining pressure increases. The explanation to this phenomenon may be the RCR specimen becomes more

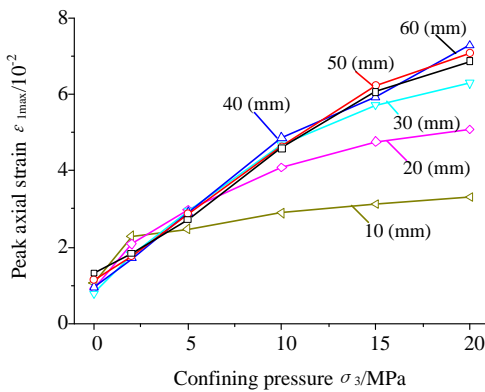


(a) Influence of confining pressure

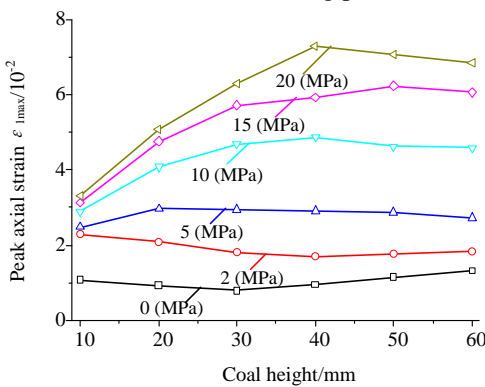


(b) Influence of coal thickness

Fig. 10 Influence of the confining pressure and coal thickness on the elastic modulus of RCR specimens



(a) Influence of confining pressure



(b) Influence of coal thickness

Fig. 11 Influence of the confining pressure and coal thickness on the peak axial strain of RCR specimens

homogenous with the increase of confining pressure.

Fig. 10(b) shows the influence of the coal thickness on the elastic modulus of RCR specimens. From Fig. 10(b), it can be seen that for the same confining pressure, the elastic modulus of RCR specimen all decreases nonlinearly as the coal thickness increases. This is because as the ratio of coal increases, the properties of RCR specimen are more similar to the coal specimens which have lower elastic modulus.

Fig. 11(a) shows the influence of the confining pressure on the peak axial strain (i.e., axial strain corresponding to the peak stress) of RCR specimens with different coal thicknesses. With the increase of the confining pressure, the peak axial strain of RCR specimen increases nonlinearly for the same coal thickness, but the increasing rate is various. The increasing rate of the peak axial strain of RCR specimen increases as the coal thickness increases until reaching 40 mm.

Fig. 11(b) shows the influence of the coal thickness on the peak axial strain of RCR specimens. As the coal thickness increases and due to the confining pressure, the peak axial strain of RCR specimen takes on a nonlinear variance. At $\sigma_3=0$ and 2 MPa, the peak axial strain decreases first and then increases as the coal thickness increases. Take $\sigma_3=2$ MPa as an example, the peak axial strain decreases from 2.2928×10^{-2} to 1.6986×10^{-2} and then increases from 1.6986×10^{-2} to 1.8274×10^{-2} with the increases of coal thickness, which has the lowest value for the coal thickness 40 mm. While at $\sigma_3=5$ MPa, the peak axial strain first increases from 2.4778×10^{-2} to 2.9688×10^{-2} and then decreases slowly from 2.9688×10^{-2} to 2.7205×10^{-2} , which is different from that at $\sigma_3=0$ and 2 MPa, and the largest value for the coal thickness 20 mm. When σ_3 ranges from 10 to 20 MPa, even though the peak axial strain also first increases and then decreases, the largest value is 40 mm or 50 mm.

3.3.3 Effects of coal thickness on the strength behavior of RCR specimens

Based on the peak stress data listed in Table 4, the influence of the confining pressure and the coal thickness on the peak stress of RCR specimens is presented in Fig. 12.

Fig. 12(a) clearly shows that there is an obvious nonlinear relation between the peak stress of RCR specimens with different coal thicknesses and the confining pressure. The peak stress increases with the increase of the confining pressure. When σ_3 increases from 0 to 10 MPa, the peak stress rapidly increases; whereas when σ_3 increases from 10 to 20 MPa, the peak stress increases slowly. Moreover, the increasing rate grows as the coal thickness of RCR specimen decreases from 60 to 10 mm when the confining pressure increases from 0 to 10 MPa, but it almost keeps steady when σ_3 is larger than 10 MPa.

From Fig. 12(b), we can conclude that at the same confining pressure, the peak stress of RCR specimens with different coal thicknesses is dependent on the coal thickness closely. At $\sigma_3=0$ MPa, the peak stress first decreases nonlinearly from 33.18 to 15.75 MPa when the coal thickness increases from 10 to 30 mm and then keeps steady when the coal thickness increases from 30 mm to 60 mm. The variation range of the peak stress is 14.02~14.79 MPa.

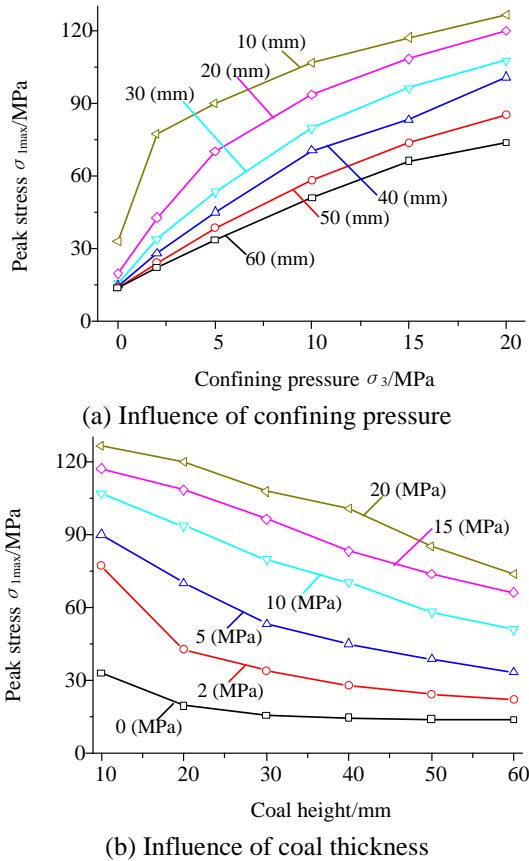


Fig. 12 Influence of the confining pressure and coal thickness on the peak stress of RCR specimens

At $\sigma_3=2$ MPa and 5 MPa, the peak stress decreases nonlinearly as the coal thickness increases from 10 to 60 mm, and the decreasing rate becomes smaller and smaller. Although the peak stress also decreases with the increase of coal thickness when σ_3 ranges from 10 to 20 MPa, the decreasing rate almost keeps stable. In brief, the peak stress decreases as the coal thickness increases for the same confining pressure.

4. Failure mechanisms of RCR specimens and discussions

Fig. 13 gives the failure modes of RCR specimens with different coal thicknesses under different confining pressures. At $\sigma_3 = 0$ MPa, the failure of RCR specimen is mainly caused by the failure of coal section, as shown in Fig. 13(a). The thinner the coal thickness is, the severer the damage of coal section is. At $\sigma_3 = 2$ MPa and 5 MPa, the failure of RCR specimen is also mainly caused by the failure of coal section except for the situation of coal thickness of 10 mm or 20 mm, as shown in Fig. 13(b) and 13(c). In a word, the failure of RCR specimen is mainly caused by the failure of the coal section under the low confining pressure condition. The explanation is that the overall loading bearing of the coal section is smaller to that of rock section, and that the failure of the coal section induces loading release for the RCR specimen. If the coal thickness is thin enough, the overall loading bearing of the

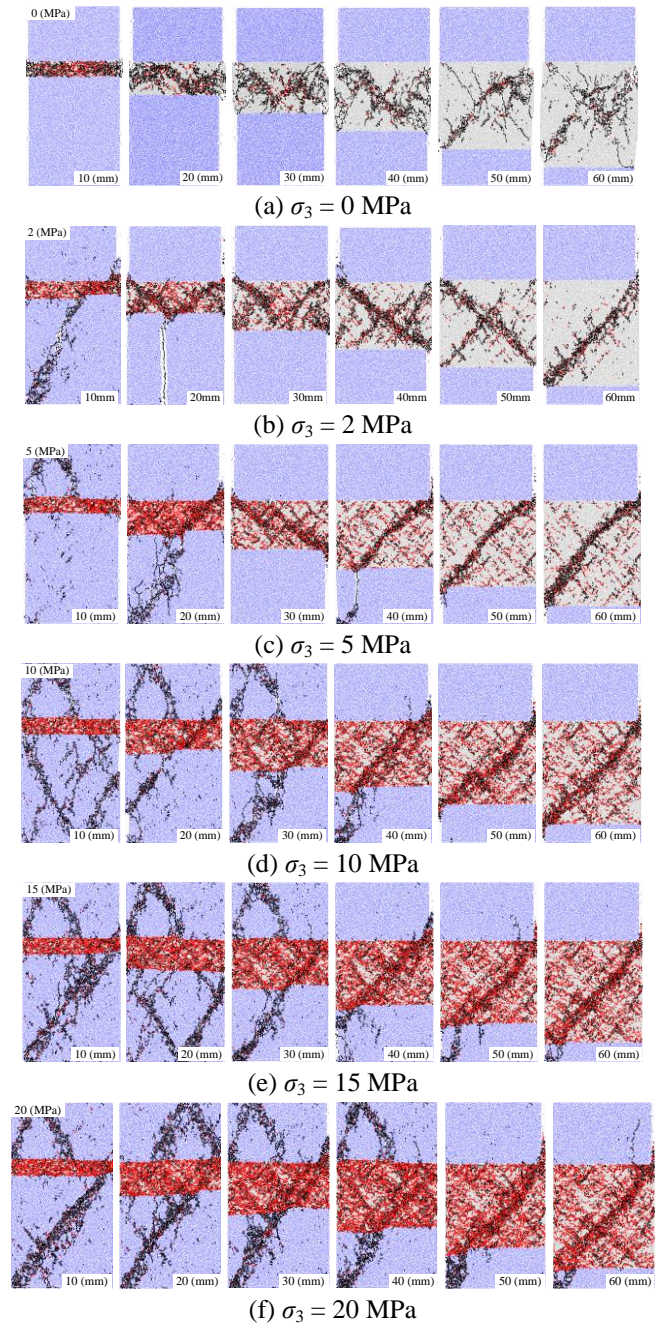


Fig. 13 Failure modes of RCR specimens with different coal thicknesses under different confining pressures (Note, the black and red dots represent the tensile micro-crack and shear micro-crack, respectively)

coal section might be enough to generate some cracks in the rock section because the bearing capacity of RCR specimen increases as the coal thickness decreases. Besides, the failure mechanism of RCR specimen is the overall failure of the coal section when the coal thickness is smaller than 30mm whereas the shear failure of the coal section when the coal thickness is larger than 30 mm. That is because if the coal thickness of RCR specimen is thick enough, the macroscopic shearing surface could form in the coal section according to Mohr-coulomb strength theory.

When σ_3 ranges from 10 to 20 MPa, the failure of RCR specimen is caused by the failure of the coal section and the

rock section, as shown in Fig. 13(d)-13(f). The reasons are as follows. First, when the coal section fractures, the released energy is enough to induce the failure of rock section for the stored energy in the specimen is high under high confining pressures. Second, the RCR specimen becomes more and more homogeneous as the confining pressure increases. In addition, when the coal thickness is larger than 30mm, obvious shear bands exist in the coal section which is similar to that under low confining pressures except that shear bands also exist in the rock section. When the coal thickness is smaller than 30 mm, the failure mechanism is the serious damage of the coal section and the shearing failure of the rock section.

5. Conclusions

In this paper, experimental investigation of uniaxial compressive tests for RCR specimens was conducted first. It shows that the overall elastic modulus and the peak stress of RCR specimens lie between the rock and the coal. On the basis of experimental tests, a systematic numerical simulation operated by PFC2D was performed to study the mechanical behavior of RCR specimens with different coal thicknesses under conventional compression tests. The main conclusions are as follows:

- In accordance with the experimental results of pure rock specimen and coal specimen, the micro-parameters simulated for RCR specimen were first confirmed. Four key factors including the stress-strain curve, the peak stress, the elastic modulus, and the failure mode, were put forward to calibrate the rightness and reasonability of micro-parameters used in the numerical simulation. We found that the numerical results were in consistent with the experimental results.

- The deformation and strength behaviors of RCR specimens depend not only on the coal thickness, but also on the confining pressure. First, the elastic modulus of RCR specimen all increase nonlinearly as the confining pressure increases, and then almost keeps steady. The elastic modulus, however, all decreases nonlinearly as the coal thickness increases under the same confining pressure. Second, the peak axial strain of RCR specimen increases nonlinearly with the increase of confining pressure. As the coal thickness increases, the peak axial strain decreases first and then increases when σ_3 is less than 5 MPa, whereas increases first and then decreases when σ_3 is larger than 5MPa. Third, the peak stress increases with an increase of the confining pressure, but the increasing rate is various for different coal thicknesses. For the same confining pressure, the peak stress also increases with the decrease of the coal thickness.

- Under low confining pressures, the failure of RCR specimen is mainly caused by the failure of the coal section. The failure mechanism of RCR specimen is the overall serious damage of coal section when the coal thickness is smaller than 30 mm, whereas when the coal thickness is larger than 30 mm, it is the shear failure of coal section. Under high confining pressures, the failure of RCR specimen is caused by the failure of coal section and rock section. Obvious shear bands exist in both the coal section

and the rock section when the coal thickness is larger than 30 mm, whereas when the coal thickness is smaller than 30 mm, the failure mechanism is the serious damage of coal section and the shearing failure of rock section.

The above conclusions mainly come from numerical simulations, which might not be the hard facts from the physical tests. However, the research of this paper reveals that the coal thickness and confining pressure have a great influence on the failure mode, the peak stress, and the elastic modulus of RCR specimen. We only simulate the failure mechanical behavior of RCR specimens with different coal thicknesses at laboratory scale, which is difficult in guiding the engineering scale directly due to obvious size effect, and therefore in the future, the scale effect of RCR mass needs to be strengthened. Besides, rock masses at depth are usually located in a triaxial stress state before excavation. The excavation of an opening disturbs the original in situ stress field, leading to stress redistribution around the excavation. If the released stress is high enough to reach the rock mass strength, the failure of rock or the rock burst will be triggered. As a result, unloading tests needs to be strengthened for researching the influence of different unloading conditions on the failure mechanical behavior of RCR specimens.

Acknowledgements

The research described in this paper was financially supported by State Key Research Development Program of China (No. 2016YFC0801401), National Natural Science Foundation of China (No. 51604165, No. 51674160, No. 51474137, and No. 51704181), Shandong Province Natural Science Foundation (No. ZR2016EEB23, and No. ZR2017BEE014), Science and Technology Program of Shandong Province University (No. J15LH02), Tai'shan Scholar Engineering Construction Fund of Shandong Province of China, Taishan Scholar Talent Team Support Plan for Advantaged & Unique Discipline Areas.

References

- Bukowska, M. (2013), "Post-peak failure modulus in problems of mining geo-mechanics", *J. Min. Sci.*, **49**(5), 731-740.
- Chen, M., Yang, S.Q., Zhang, Y.C. and Zang, C.W. (2016), "Analysis of the failure mechanism and support technology for the Dongtan deep coal roadway", *Geomech. Eng.*, **11**(3), 401-420.
- Chen, X., Liao, Z.H. and Peng, X. (2012), "Deformability characteristics of jointed rock masses under uniaxial compression", *Int. J. Min. Sci. Technol.*, **22**(2), 213-221.
- Duncan, J.M. (2000), "Factors of safety and reliability in geotechnical engineering", *J. Geotech. Geoenviron. Eng.*, **126**(4), 307-316.
- Gale, W.J. (1998), "Coal pillar design issues in longwall mining", Ph.D. Dissertation, University of Wollongong and The Australasian Institute of Mining and Metallurgy, Wollongong, Australia.
- Guo, D.M., Zuo, J.P., Zhang, Y. and Yang, R.S. (2011), "Research on strength and failure mechanism of deep coal-rock combination bodies of different inclined angles", *Rock Soil Mech.*, **32**(5), 1333-1339 (in Chinese).

- Guo, W.Y., Tan, Y.L., Yang, Z.L., Zhao, T.B. and Hu, S.C. (2017b), "Effect of saturation time on the bursting liability indexes of coal and its application for rock burst mitigation", *Geotech. Geol. Eng.*, **36**(1), 589-597.
- Guo, W.Y., Zhao, T.B., Tan, Y.L., Yu, F.H., Hu, S.C. and Yang, F.Q. (2017a), "Progressive mitigation method of rock bursts under complicated geological conditions", *Int. J. Rock Mech. Min. Sci.*, **96**, 11-22.
- He, X.Q., Chen, W.X., Nie, B.S. and Mitri, H.N. (2011), "Electromagnetic emission theory and its application to dynamic phenomena in coal-rock", *Int. J. Rock Mech. Min. Sci.*, **48**(8), 1352-1358.
- Huang, B.X. and Liu, J.W. (2013), "The effect of loading rate on the behavior of samples composed of coal and rock", *Int. J. Rock Mech. Min. Sci.*, **61**(10), 23-30.
- Huang, W.P., Yuan, Q., Tan, Y.L., Wang, J., Liu, G.L., Qu, G.L. and Li, C. (2017), "An innovative support technology employing a concrete-filled steel tubular structure for a 1000-m-deep roadway in a high in situ stress field", *Tunn. Undergr. Sp. Technol.*, **73**, 26-36.
- Kaiser, P.K. and Cai, M. (2012), "Design of rock support system under rockburst condition", *J. Rock Mech. Geotech. Eng.*, **4**(3), 215-227.
- Lin, H. and Chen, J.Y. (2017), "Back analysis method of homogeneous slope at critical state", *KSCE J. Civ. Eng.*, **21**(3), 670-675.
- Lin, H., Zhong, W.W. and Cao, P. (2016), "Three-dimensional rock slope stability analysis considering the surface load distribution", *Eur. J. Environ. Civ. Eng.*, **20**(8), 877-898.
- Liu, C.L., Tan, Z.X., Deng, K.Z. and Li, P.X. (2013), "Synergistic instability of coal pillar and roof system and filling method based on plate model", *Int. J. Min. Sci. Technol.*, **23**(1), 145-149.
- Lu, C.P., Liu, G.J., Liu, Y., Zhang, N., Xue, J.H. and Zhang, L. (2015), "Microseismic multi-parameter characteristics of rockburst hazard induced by hard roof fall and high stress concentration", *Int. J. Rock Mech. Min. Sci.*, **76**, 18-32.
- Meng, F.Z., Zhou, H., Zhang, C.Q., Xu, R.C. and Lu, J.J. (2015), "Evaluation methodology of brittleness of rock based on post-peak stress-strain curves", *Rock Mech. Rock Eng.*, **48**(5), 1787-1805.
- Newman, D.A. (2002), "A case history investigation of two coal bumps in the southern appalachian coalfield", *Proceedings of the 21st International Conference on Ground Control in Mining*, Morgantown, West Virginia, U.S.A.
- Ning, J.G., Wang, J., Jiang, J.Q., Hu, S.C., Jiang, L.S. and Liu, X.S. (2017), "Estimation of crack initiation and propagation thresholds of confined brittle coal specimens based on energy dissipation theory", *Rock Mech. Rock Eng.*, **51**(1), 119-134.
- Panaghi, K., Golshani, A. and Takemura, T. (2015), "Rock failure assessment based on crack density and anisotropy index variations during triaxial loading tests", *Geomech. Eng.*, **9**(6), 793-813.
- Potyondy, D.O. and Cundall, P.A. (2004), "A bonded-particle model for rock", *Int. J. Rock Mech. Min. Sci.*, **41**(8), 1329-1364.
- Poulsen, B.A., Shen, B., Williams, D.J., Huddleston-Holmes, C., Erarslan, N. and Qin, J. (2014), "Strength reduction on saturation of coal and coal measures rocks with implications for coal pillar strength", *Int. J. Rock Mech. Min. Sci.*, **71**, 41-52.
- Rodríguez, R. and Lombardía, C. (2010), "Analysis of methane emissions in a tunnel excavated through Carboniferous strata based on underground coal mining experience", *Tunn. Undergr. Sp. Technol.*, **25**(4), 456-468.
- Sherizadeh, T. and Kulatilake, P.H. (2016), "Assessment of roof stability in a room and pillar coal mine in the U.S. using three-dimensional distinct element method", *Tunn. Undergr. Sp. Technol.*, **59**, 24-37.
- Song, D.Z., Wang, E.Y., Xu, J.K., Liu, X.F., Shen, R.X. and Xu, W.Q. (2015), "Numerical simulation of pressure relief in hard coal seam by water jet cutting", *Geomech. Eng.*, **8**(4), 495-510.
- Takeuchi, A., Lau, W.S. and Freund, F.T. (2006), "Current and surface potential induced by stress-activated positive holes in igneous rocks", *Phys. Chem. Earth*, **31**(4-9), 240-247.
- Tan, Y.L., Guo, W.Y., Gu, Q.H., Zhao, T.B., Yu, F.H., Hu, S.C. and Yin, Y.C. (2016), "Research on the rockburst tendency and AE characteristics of inhomogeneous coal-rock combination bodies", *Shock Vib.*, (2), 1-11.
- Tan, Y.L., Liu, X.S., Ning, J.G. and Lu, Y.W. (2017), "In situ investigations on failure development of overlying strata induced by mining multiple coalseams", *Geotech. Test. J.*, **40**(2), 244-257.
- Tan, Y.L., Yu, F.H., Ning, J.G. and Zhao, T.B. (2015), "Design and construction of entry retaining wall along a gob side under hard roof stratum", *Int. J. Rock Mech. Min. Sci.*, **77**, 115-121.
- Vakili, A. and Hebblewhite, B.K. (2010), "A new cavability assessment criterion for longwall top coal caving", *Int. J. Rock Mech. Min. Sci.*, **47**(8), 1317-1329.
- Wang, G., Pan, Y.S., Xiao, X.C., Wu, D., Ding, X. and Zhao, X. (2016), "Experimental study on charge law of coal-rock bodies rock burst tendency and failure characteristics", *Chin. Safety Sci. J.*, **26**(7), 135-140 (in Chinese).
- Wang, T., Jiang, Y.D., Zhan, S.L. and Wang, C. (2014), "Frictional sliding tests on combined coal-rock samples", *J. Rock Mech. Geotech. Eng.*, **6**(3), 280-286.
- Zhang, G.C., Liang, S.J., Tan, Y.L., Xie, F.X., Chen, S.J. and Jia, H.G. (2018), "Numerical modeling for longwall pillar design: A case study from a typical longwall panel in China", *J. Geophys. Eng.*, **15**(1), 121-134.
- Zhang, X.P. and Wong, L.N.Y. (2013), "Loading rate effects on cracking behavior of flaw-contained specimens under uniaxial compression", *Int. J. Fracture*, **180**(1), 93-110.
- Zhang, X.P., Jiang, Y.J., Wang, G., Wang, J.C., Wu, X.Z. and Zhang, Y.Z. (2016), "Numerical experiments on rate-dependent behaviors of granite based on particle discrete element model", *Rock Soil Mech.*, **37**(9), 2679-2685.
- Zhang, Z.T., Liu, J.F., Wang, L., Yang, H.T. and Zuo, J.P. (2012), "Effects of combination mode on mechanical properties and failure characteristics of the coal-rock combinations", *J. Chin. Coal Soc.*, **37**(10), 1677-1681 (in Chinese).
- Zhao, T.B., Guo, W.Y., Lu, C.P. and Zhao, G.M. (2016), "Failure characteristics of combined coal-rock with different interfacial angles", *Geomech. Eng.*, **11**(3), 345-359.
- Zhao, T.B., Guo, W.Y., Tan, Y.L., Lu, C.P. and Wang, C.W. (2017a), "Case histories of rock bursts under complicated geological conditions", *Bull. Eng. Geol. Environ.*, 1-17.
- Zhao, T.B., Guo, W.Y., Tan, Y.L., Yin, Y.C., Cai, L.S. and Pan, J.F. (2018), "Case studies of rock bursts under complicated geological conditions during multi-seam mining at a depth of 800 m", *Rock Mech. Rock Eng.*, **51**(5), 1539-1564.
- Zhao, T.B., Guo, W.Y., Tan, Y.L., Yu, F.H., Huang, B. and Zhang, L.S. (2017b), "Failure mechanism of layer-crack rock models with different vertical fissure geometric configurations under uniaxial compression", *Adv. Mech. Eng.*, **9**(11), 1-15.
- Zhao, W.H., Huang, R.Q. and Yan, M. (2015b), "Mechanical and fracture behavior of rock mass with parallel concentrated joints with different dip angle and number based on PFC simulation", *Geomech. Eng.*, **8**(6), 757-767.
- Zhao, Z.H., Wang, W.M., Wang, L.H. and Dai, C.Q. (2015a), "Compressive-shear strength criterion of coal-rock combination model considering interface effect", *Tunn. Undergr. Sp. Technol.*, **47**, 193-199.
- Zuo, J.P., Wang, Z.F., Zhou, H.W., Pei, J.L. and Liu, J.F. (2013), "Failure behavior of a RCR combined body with a weak coal interlayer", *Int. J. Min. Sci. Technol.*, **23**(6), 907-912.

Zuo, J.P., Xie, H.P., Wu, A.M. and Liu, J.F. (2011), "Investigation on failure mechanisms and mechanical behaviors of deep coal-rock single body and combined body", *Chin. J. Rock Mech. Eng.*, **30**(1), 84-92 (in Chinese).

CC